

https://dspace.org/

Multiple slip effects with Hall current on the threedimensional hybrid nanofluid flow combining dissipative heat impact over a slandering surface

S Panda; F Oluwaseun; Titilayo Agbaje; R Baithalu; S Mishra

https://hdl.handle.net/10539/47312
WOS

Downloaded from a DSpace repository. https://dspace.org/

Journal of Thermal Analysis and Calorimetry (2025) 150:11293–11304
https://doi.org/10.1007/s10973-025-14440-0

Multiple slip effects with Hall current on the three-dimensional hybrid nanofluid flow combining dissipative heat impact over a slandering surface

Subhajit Panda[1] · Folarin Oluwaseun[2] · Titilayo M. Agbaje[2] · Rupa Baithalu[3] · S. R. Mishra[3]

Received: 10 January 2025 / Accepted: 18 May 2025 / Published online: 28 June 2025
© Akadémiai Kiadó Zrt 2025

Abstract

The advanced heat transfer properties of various nanofluids are beneficial for the production processes in the current need of science and technology. The significant contribution of enhanced thermal properties is due to the involvement of the particle concentrations, shape and size of the nanoparticles. The recent investigation based on the utility of the magnetic nanoparticles such as Fe_3O_4 combined with titanium oxide (TiO_2) in the base liquid ethylene glycol hybridized fluid movement via an expanding/contracting slandering surface. The flow over the elongating surface packed with permeable medium enriches the flow characteristic. The flow characteristic is enhanced for the interpretation of both the Joule and Darcy dissipation and the impact of multiple slip that is assumed as surface condition. The mathematical model equipped with the aforementioned assumptions gets converted into dimensionless form by the utilization of similarity rules and the proposed model is tackled numerically using shooting-based Runge–Kutta technique. Further, the detailed discussion on the physical properties of several factors is presented briefly via a validation with earlier investigation.

Keywords Magnetic nanoparticle · Ethylene glycol-based hybrid nanofluid · Hall current · Joule and Darcy dissipation · Velocity and thermal slip · Numerical method

Introduction

Hybrid nanofluids, created by dispersing two or more different types of nanoparticles within a base fluid, have shown great potential for improving thermal performance beyond that of traditional single-component nanofluids. The combined thermal and physical characteristics of multiple nanoparticles enable these fluids to exhibit higher thermal conductivity, increased stability, and improved viscosity control. Such advantages make hybrid nanofluids suitable for demanding heat transfer applications, including advanced cooling technologies, heat exchangers, and solar thermal systems. Research indicates that the interaction between different nanoparticles can significantly boost convective heat transfer, particularly when guided by statistical or computational optimization methods. Consequently, hybrid nanofluids hold considerable potential for improving thermal efficiency across a broad range of industrial and engineering systems. Almheidat et al. [1] conducted a nanoscale heat transport analysis of a magnetized trihybrid nanofluid flowing over a wedge-shaped artery using a combination of the Keller box and finite element methods. They also examined

✉ S. R. Mishra
satyaranjan_mshr@yahoo.co.in

Subhajit Panda
spanda.math@gmail.com

Folarin Oluwaseun
folarino987@yahoo.com

Titilayo M. Agbaje
titilayoagbaje@gmail.com

Rupa Baithalu
rupadhananjaygarnaik@gmail.com

[1] Centre for Data Science, Siksha 'O' Anusandhan Deemed to be University, Bhubaneswar, Odisha 751030, India

[2] School of Computer Science and Applied Mathematics, University of the Witwatersrand, Private Bag 3, Braamfontein, Johannesburg 2050, South Africa

[3] Department of Mathematics, Siksha 'O' Anusandhan Deemed to be University, Bhubaneswar, Odisha 751030, India

the influence of nonlinear radiation on a magneto-Casson woodworm fluid containing hybrid nanomaterials dispersed in sodium alginate, with applications in smart textiles. The study provides a comparative evaluation of thermal performance between mono-nanomaterials and hybrid nanofluids. Also, a reduction in velocity with increasing magnetic parameter is observed for both hybrid and mono nanofluids, with the decline being more pronounced in hybrid nanofluids. Additionally, the stagnation point parameter is shown to significantly influence the velocity for both types of nanofluids. The application of hybridized fluids in wavy channels under the influence of entropy generation was discussed by Abderrahmane et al. [2]. Their work uses the "Galerkin finite element method (FEM)" to solve a numerical result for buoyancy-driven flow of nanofluids in a cavity with a magnetic field. They showed that heat transfer efficiency is positively impacted when non-Newtonian nanofluids are combined with porous media. Similarly, Zhu et al. [3] anticipated the thermal performance of antifreeze hybrid nanoparticles, highlighting their utility in thermal applications. Ibrahim et al. [4] examined dissipative MHD Casson fluid flow over a porous, exponentially stretching surface, accounting for heat generation, suction/injection, radiation, and reactive species. Reddy et al. [5] applied a finite discretization method to study unsteady MHD oscillatory mixed convective movement induced by an oscillating plate, considering both chemical species and thermal radiation. Yun-Xiang Li et al. [6] provided a computational analysis of the unsteady MHD nanofluid transportation, incorporating thermal and mass attributes, chemical reactions, and the interaction of a heat source. Zainal et al. [7] examined temperature circulation in a hybrid nanofluid through a porous, moving wedge, considering bimolecular reaction and a binary chemical reaction. Almaneea [8] performed a numerical investigation on the improvement of thermo-solutal attributes in MHD Williamson fluid incorporating hybrid nanoparticles under both catalytic reactions. Hussain et al. [9] analyzed the interpretation of a first-order chemical reaction and melting heat on the flow of a hybrid nanoliquid over a nonlinearly stretched curved surface with shape factors. Suneetha et al. [10] analyzed the influence of thermal radiation on unsteady hydromagnetic free convection movement past a vertically aligned plate that was impulsively started. Their study accounted for spatial variations in both surface temperature and solutal concentration, emphasizing the transient behavior of the flow under electromagnetic and radiative effects. In a related investigation, Ogulu and Makinde [11] examined the transient magnetically free convection flow of a viscous, radiative fluid along a vertical plate subjected to a constant heat flux. Their work highlighted the combined influence of radiative heat transfer and magnetic fields on the thermal and velocity profiles. Trishivi et al. [12] investigated the movement of a copper–water nanofluid over an exponentially elastic slippery surface, incorporating key physical parameters into the model. The outcomes are extensively illustrated and discussed to offer detailed insight. Moreover, computational results for engineering-relevant physical quantities are presented and analyzed. Sarma et al. [13] reported the dynamics of a Jeffrey hybrid nanofluid (TiO_2–Cu/H_2O) flowing over a porous medium embedded in an exponentially stretching surface. The nonlinear governing equations were solved using MATLAB's bvp4c solver, accounting for various influential parameters. Additionally, Hamad [14] explored the imposition of an external magnetism on the stability and convective behavior of a nanofluid flowing over a vertical surface, highlighting the complex interplay between magnetohydrodynamics and natural convection in porous environments. Reddy et al. [15] conducted a comprehensive study on the magnetohydrodynamic (MHD) stagnation point flow of a Williamson hybrid nanofluid via an elastic material embedded in a porous medium. Their research focused on analyzing the combined effects of various physical phenomena, including heat generation and chemical reactions, on the flow characteristics. Sharma and Mishra [16] analyzed radiative heat and solutal concentration effects in the convective flow of a polar fluid over a stretching surface, highlighting the influence of Soret and magnetization phenomena. Malik et al. [17] examined the MHD behavior of a tangentially oriented hyperbolic fluid flowing over a stretched cylinder using the "Keller Box scheme." Akbar et al. [18] deliberated the motion of a hyperbolic fluid over a magnetohydrodynamic boundary layer stretched surface via numerical techniques. Idowu et al. [19] anticipated the MHD thermo-solutal characteristics of Casson fluid under the effects of variable viscosity and thermal conductivity. Gbadeyan et al. [20] explored how changes in heat transfer efficiency and viscosity influence Casson nanofluid flow with convective heating and velocity slip. Reddy and Naik [21] addressed MHD convective flow of Casson nanofluid over an exponentially inclined, stretching surface embedded in a porous medium, incorporating radiative heat, internal heat generation, and Ohmic dissipation. By applying similarity transformations, the governing PDEs were reduced to ODEs and solved using MATLAB's built-in *bvp4c* solver.

Goal of the proposed investigation: The current investigation aims to;

- Explore the analysis of hybrid nanofluid flow composed of magnetic nanoparticle like Fe_3O_4 with TiO_2 in EG over a slandering surface packed with porous medium.
- Examine the role of adopted thermal attributes such as thermal conductivity, electrical conductivity, and viscosity of hybrid nanofluid in association with the impact of solid nanoparticles.
- Execute the interpretation of Hall current considering the insertion of dissipative heat in the energy equation.

- Project the role of velocity and thermal slip at the surface of the fluid which affect the flow behavior.

Novelty: This study is distinguished by the following novel features:

- The assumption of magnetic nanoparticles such as Fe_3O_4 combined with TiO_2 nanoparticles in EG-base liquid performs a greater control of fluid flow.
- The bi-hybrid nanofluid flow over a slandering surface embedding within permeable medium is useful in designing the wing structure of aircraft.
- For the enhanced heat transport properties the role of Hall current along with nonlinear buoyancy is vital.
- The dissipative heat for the combined impact of Joule and Darcy dissipation enriches the heat transportation mechanism.
- The role of all the above assumptions is important in targeted drug delivery, cancer therapy, etc.

Model formulation

An assessment is proposed for the movement of bi-hybrid nanofluid composed of Fe_3O_4, a magnetized nanoparticle and titanium oxide TiO_2 in the base liquid ethylene glycol through a slandering surface. The medium is saturated with a porous matrix. The main emphasis of the investigation is the impact of multiple slip those are applied at the surface conditions. The heat transfer process is examined, taking into account for the dissipative heat such as viscous and Joule effect associated with the Hall current effect. In particular, the flow is confined within $z \geq 0$ region, whereas the magnetic field is imposed along the z-direction. The surface velocity of the extending surfaces along the $xy-$ plane is $u_w = u_0(b+y+x)^n$,and $v_w = v_0(b+y+x)^n$ respectively. The assumption for the wall temperature vis-à-vis the ambient state temperature are considered as T_w and T_∞, respectively (Fig. 1).

However, the major assumptions are;

- The impact of Hall current along with nonlinear buoyancy in the fluid velocity.
- The slandering sheet embedding with porous matrix.
- Dissipative heat integrated with the role of Joule and Darcy effect.
- Assumption of velocity and thermal slip.

Pertaining to the aforesaid assumptions the flow phenomena of the proposed fluid is mentioned as;

$$\frac{\partial u}{\partial x}+\frac{\partial v}{\partial y}+\frac{\partial w}{\partial z}=0, \tag{1}$$

$$u\frac{\partial u}{\partial x}+v\frac{\partial u}{\partial y}+w\frac{\partial u}{\partial z}=\upsilon_{\mathrm{hnf}}\frac{\partial^2 u}{\partial z^2}-\frac{\sigma_{\mathrm{hnf}}B^2}{\rho_{\mathrm{hnf}}\left(1+m^2\right)}(u+mv)-\frac{\mu_{\mathrm{hnf}}}{\rho_{\mathrm{hnf}}k_{\mathrm{p}}^*}u, \tag{2}$$

$$u\frac{\partial v}{\partial x}+v\frac{\partial v}{\partial y}+w\frac{\partial v}{\partial z}=\upsilon_{\mathrm{hnf}}\frac{\partial^2 v}{\partial z^2}-\frac{\sigma_{\mathrm{hnf}}B^2}{\rho_{\mathrm{hnf}}\left(1+m^2\right)}(v-mu)-\frac{\mu_{\mathrm{hnf}}}{\rho_{\mathrm{hnf}}k_{\mathrm{p}}^*}v, \tag{3}$$

$$\begin{aligned}u\frac{\partial T}{\partial x}+v\frac{\partial T}{\partial y}+w\frac{\partial T}{\partial z}&=\alpha_{\mathrm{hnf}}\frac{\partial^2 T}{\partial z^2}+\frac{\sigma_{\mathrm{hnf}}B^2}{(\rho Cp)_{\mathrm{hnf}}\left(1+m^2\right)}\left(u^2+v^2\right)\\&+\frac{\mu_{\mathrm{hnf}}}{(\rho Cp)_{\mathrm{hnf}}}\left(\left(\frac{\partial u}{\partial z}\right)^2+\left(\frac{\partial v}{\partial z}\right)^2\right)\\&+\frac{\mu_{\mathrm{hnf}}}{(\rho Cp)_{\mathrm{hnf}}k_{\mathrm{p}}^*}\left(u^2+v^2\right)+\frac{Q^*(T-T_\infty)}{(\rho Cp)_{\mathrm{hnf}}}.\end{aligned} \tag{4}$$

The corresponding surface conditions reported as

$$\left.\begin{aligned}&u=h_1^*\frac{\partial u}{\partial z}+u_{\mathrm{w}},v=h_1^*\frac{\partial v}{\partial z}+v_{\mathrm{w}},w=0,T=h_2^*\frac{\partial T}{\partial z}+T_{\mathrm{w}},\\&u\to 0,T\to T_\infty,v\to 0,\end{aligned}\right\} \tag{5}$$

$$z=j(b+x+y)^{\frac{1-n}{2}}.$$

The followings are the similarity rules utilized for the transformation of the non-dimensional model:

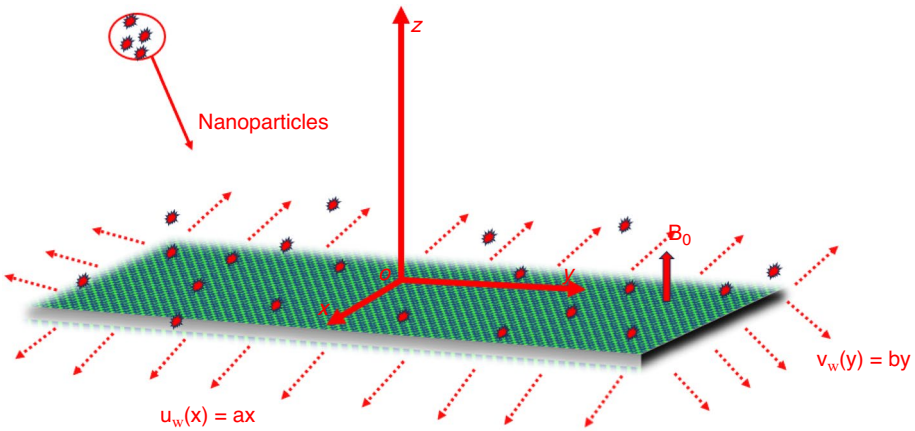


Fig. 1 Flow geometry

$$\left.\begin{aligned} &u = u_0(b+y+x)^{\mathrm{n}}F'(\eta), \eta = z\left(\frac{u_0}{\upsilon_f}\right)^{1/2}(b+y+x)^{\frac{\mathrm{n}-1}{2}},\\ &v = u_0(b+y+x)^{\mathrm{n}}G'(\eta), T - T_\infty = \left(T_{\mathrm{w}} - T_\infty\right)\theta(\eta),\\ &w = -\left(u_0\upsilon_{\mathrm{f}}\right)^{1/2}(b+y+x)^{\frac{\mathrm{n}-1}{2}}\left(\frac{n+1}{2}(F(\eta)+G(\eta)) - \eta\frac{1-n}{2}\left(F'(\eta)+G'(\eta)\right)\right), \end{aligned}\right\}. \tag{6}$$

The wall velocity, temperature corresponds to,

$$\left.\begin{aligned} &u_{\mathrm{w}} = u_0(b+y+x)^{\mathrm{n}}, v_{\mathrm{w}} = u_0(b+y+x)^{\mathrm{n}}T_{\mathrm{w}} = T_\infty + T_0(b+y+x)^{\frac{1-\mathrm{n}}{2}},\\ &B = B_0(b+y+x)^{\frac{1-\mathrm{n}}{2}}, \Lambda^2 = K_0^2(b+y+x)^{\mathrm{n}-1}. \end{aligned}\right\} \tag{7}$$

Using the above-mentioned similarity rules the model presented in Eqs. (2)–(10) are transformed to,

$$F''' + \chi_1\chi_2\frac{(n+1)(F+G)}{2}F'' - \frac{\mathrm{Ha}^2\chi_2\chi_3}{(1+m)^2}\left(F'+mG'\right) - \chi_1\chi_2\left(nF'+nG'\right)F' - \mathrm{Da}F' = 0 \tag{8}$$

$$G''' + \chi_1\chi_2\left(\frac{n+1}{2}\right)\left(\frac{F+G}{2}\right)G'' + \frac{\mathrm{Ha}^2\chi_2\chi_3}{(1+m)^2}\left(mF'-G'\right) - n\chi_1\chi_2\left(F'+G'\right)G' - \mathrm{Da}G' = 0 \tag{9}$$

$$\chi_5\theta'' + \mathrm{Pr}\,Ec\left(F'^2+G'^2\right)\left(\chi_3\frac{\mathrm{Ha}^2}{\left(1+m^2\right)} + \chi_1\mathrm{Da}\right) + \chi_1\,\mathrm{Pr}\,\mathrm{Ec}\left(F''^2+G''^2\right) + \chi_4\,\mathrm{Pr}\,(F+G)\theta' + \mathrm{Pr}\,Q\theta = 0. \tag{10}$$

The surface conditions are conveniently expressed as:

$$\left.\begin{aligned} &\left(\begin{aligned} &F = \alpha_1\left(\tfrac{1-n}{1+n}\right)\left(1+K_1F''\right), G = \alpha_1\left(\tfrac{1-n}{1+n}\right)\left(1+K_1G''\right), F' = K_1F''+1,\\ &G' = K_1G'' + A, \theta = K_2\theta' + 1. \end{aligned}\right) \text{ at } \eta \to \alpha_1\\ &F' \to 0, G' \to 0, \theta \to 0, \qquad \text{at } \eta \to \infty. \end{aligned}\right. \tag{11}$$

Further, the domain defined on [0, ∞) urge to introduce the transformed functions,

$$\begin{pmatrix} F(\eta) = f\left(\eta-\alpha_1\right) = f(\zeta), G(\eta) = g\left(\eta-\alpha_1\right) = g(\zeta)\\ \theta(\eta) = \theta\left(\eta-\alpha_1\right) = \theta(\zeta). \end{pmatrix} \tag{12}$$

Using the similarity transformation, Eq. (2–5) takes the subsequent forms,

$$f''' + \chi_1\chi_2\left(\frac{n+1}{2}\right)\left(\frac{f+g}{2}\right)f'' - \frac{\mathrm{Ha}^2\chi_2\chi_3}{(1+m)^2}\left(f'+mg'\right) - \chi_1\chi_2\left(nf'+ng'\right)f' - \mathrm{Da}\,f' = 0 \tag{13}$$

$$g''' + \chi_1\chi_2\left(\frac{n+1}{2}\right)\left(\frac{f+g}{2}\right)g'' + \frac{\mathrm{Ha}^2\chi_2\chi_3}{(1+m)^2}\left(mf'-g'\right) - n\chi_1\chi_2\left(f'+g'\right)g' - \mathrm{Da}\,g' = 0 \tag{14}$$

$$\chi_5\theta'' + \mathrm{Pr}\,\mathrm{Ec}\left(f'^2+g'^2\right)\left(\chi_3\frac{\mathrm{Ha}^2}{\left(1+m^2\right)} + \chi_1\mathrm{Da}\right) + \chi_1\,\mathrm{Pr}\,\mathrm{Ec}\left(f''^2+g''^2\right) + \chi_4\,\mathrm{Pr}\,(f+g)\theta' + \mathrm{Pr}\,Q\theta = 0. \tag{15}$$

The corresponding boundary condition is expressed as follows:

$$\left.\begin{aligned} &\left(\begin{aligned} &f = \left(\tfrac{1-n}{1+n}\right)\left(\alpha_1+\alpha_1K_1f''\right), g = \left(\tfrac{1-n}{1+n}\right)\left(\alpha_1+\alpha_1K_1g''\right), f' = 1+K_1f'',\\ &g' = K_1g'' + A, \theta = K_2\theta' + 1. \end{aligned}\right) \text{ at } \eta \to \alpha_1\\ &f' \to 0, g' \to 0, \theta \to 0, \qquad \text{at } \eta \to \infty. \end{aligned}\right. \tag{16}$$

The emerging parameters are characterized by Ha^2 Hartmann number, Ec, Eckert number, Pr Prandtl number, and α_1 wall thickness factor separately. Further, K_1, K_2, are velocity and thermal slip constraints. The expression for the parameters used in the flow phenomena are,

$$\left.\begin{array}{l}\delta=\frac{T_w}{T_\infty},\alpha_1=j\sqrt{\frac{u_0}{\upsilon_f}},E=\frac{E_a}{T_\infty k_1^*},K_r=\frac{K_0^2}{u_0},\mathrm{Ha}^2=\frac{\sigma_f B_0^2}{u_0\rho_f},\\ \mathrm{Da}=\frac{\upsilon^2}{k_p^* u_0^2},\mathrm{Ec}=\frac{u_w^2}{(Cp)_f(T_w-T_\infty)},\mathrm{Pr}=\frac{\upsilon_f}{\alpha},\mathrm{Sc}=\frac{\upsilon_f}{D_B},Q=\frac{Q^*}{u_0(\rho Cp)_f}\\ K_1=h_1^*\sqrt{\frac{u_0}{\upsilon}}(b+x+y)^{\frac{n-1}{2}},K_2=h_2^*(T_w-T_\infty)\sqrt{\frac{u_0}{\upsilon}}(b+x+y)^{\frac{n-1}{2}}\end{array}\right\}. \tag{17}$$

The constants defined for the thermal models used in the governing equation are;

Viscosity model:

$$\chi_1=\frac{\mu_{hnf}}{\mu_f}=\frac{1}{(1-\phi_1)^{2.5}(1-\phi_2)^{2.5}}.$$

Density model:

$$\chi_2=\frac{\rho_{hnf}}{\rho_f}=(1-\phi_2)\left[(1-\phi_1)+\phi_1\frac{\rho_{s1}}{\rho_f}\right]+\phi_2\frac{\rho_{s2}}{\rho_f}.$$

Electrical conductivity model:

$$\chi_3=\frac{\sigma_{hnf}}{\sigma_{nf}}\times\frac{\sigma_{nf}}{\sigma_f}$$

$$\frac{\sigma_{s2}+(n-1)\sigma_{nf}-(n-1)\phi_2(\sigma_{nf}-\sigma_{s2})}{\sigma_{s2}+(n-1)\sigma_{nf}+\phi_2(\sigma_{nf}-\sigma_{s2})}\times\frac{\sigma_{s1}+(n-1)\sigma_f-(n-1)\phi_1(\sigma_f-\sigma_{s1})}{\sigma_{s1}+(n-1)\sigma_f+\phi_1(\sigma_f-\sigma_{s1})}.$$

Specific heat model:

$$\chi_4=\frac{(\rho Cp)_{hnf}}{(\rho Cp)_f}=\phi_2\frac{(\rho Cp)_{s2}}{(\rho Cp)_f}+(1-\phi_2)\left[(1-\phi_1)+\phi_1\frac{(\rho Cp)_{s1}}{(\rho Cp)_f}\right].$$

Thermal conductivity model:

$$\chi_5=\frac{k_{hnf}}{k_{nf}}\times\frac{k_{nf}}{k_f}$$

$$\frac{k_{s2}+(n-1)k_{nf}-(n-1)\phi_2(k_{nf}-k_{s2})}{k_{s2}+(n-1)k_{nf}+\phi_2(k_{nf}-k_{s2})}\times\frac{k_{s1}+(n-1)k_f-(n-1)\phi_1(k_f-k_{s1})}{k_{s1}+(n-1)k_f+\phi_1(k_f-k_{s1})}.$$

Physical quantities:

The physical quantities, such as friction drag and heat transport rate, hold significant value from an engineering perspective. These quantities of interest are mathematically defined as follows:

$$Cf_x=\frac{\tau_{xz}}{u_w^2\rho_f},Cf_y=\frac{\tau_{yz}}{v_w^2\rho_f},\mathrm{Nu}_x=\frac{(x+y+b)q_m}{k_f(T_w-T_\infty)}. \tag{18}$$

In general, τ_{xz}, τ_{yz}, and q_m, are defined as,

$$\tau_{xz}=\mu_{hnf}\left|\frac{\partial u}{\partial z}\right|_{z=j(b+y+x)^{\frac{1-n}{2}}},\tau_{xz}=\mu_{hnf}\left|\frac{\partial v}{\partial z}\right|_{z=j(b+y+x)^{\frac{1-n}{2}}},q_m=-\left|k_{hnf}\frac{\partial T}{\partial z}\right|_{z=j(b+y+x)^{\frac{1-n}{2}}} \tag{19}$$

In their dimensionless form, these equations are expressed as:

$$\begin{aligned}&(\mathrm{Re}_x)^{0.5}Cf_x=2\left(\frac{n+1}{2}\right)^{0.5}\chi_1 f''(0),(\mathrm{Re}_y)^{0.5}Cf_y\\&=2\left(\frac{n+1}{2}\right)^{0.5}\chi_1 g''(0),\\&\mathrm{Nu}_x(\mathrm{Re}_x)^{-0.5}=-\left(\frac{n+1}{2}\right)^{0.5}\chi_5\theta'(0),\end{aligned} \tag{20}$$

$$\mathrm{Re}_x=\frac{(b+y+x)u_w}{\upsilon},\mathrm{Re}_y=\frac{(b+y+x)v_w}{\upsilon}.$$

Discussion following validation

The present investigation aims the numerical investigation on the ethylene glycol-based hybrid nanofluid composed of Fe_3O_4 and TiO_2 nanoparticles over an extended surface for the impact of dissipative heat embedding within a permeable medium. The impact of Hall current with an additional heat source enriches the heat transport phenomenon. Table 1 presents the thermal attributes of Fe_3O_4 and TiO_2 combined with base liquid EG in a standard temperature collected from

Table 1 Thermophysical features of the base fluid and nanoparticles

Particles and base liquid	ρ/Kg m^{-3}	k/W m^{-1} K^{-1}	c_p/J Kg^{-1} K^{-1}	σ/S m^{-1}
Titanium dioxide (TiO_2)	4250	8.9538	686.2	2.38×10^6
Cobalt Ferrite (Fe_3O_4)	4907	3.7	700	5.51×10^9
Ethylene Glycol($C_2H_6O_2$)	1113.5	0.253	2347	4.3×10^{-5}

Table 2 Comparison of w ith $f''(0)$ with previously reported findings for Ha $= \alpha_1 = K_1 = K_2 = Q = m = \phi_1 = \phi_2 = 0$

n	A	Xia et al. [22] $f''(0)$	Present study $f''(0)$
1.0	0.0	−1.000008	−1.000008233
	0.5	−1.224780	−1.224755245
1.0	1.0	−1.414424	−1.414421467
3.0	0.0	−1.624355	−1.624357134
3.0	0.5	−1.989425	−1.989423456
3.0	1.0	−2.2297186	−2.229718245

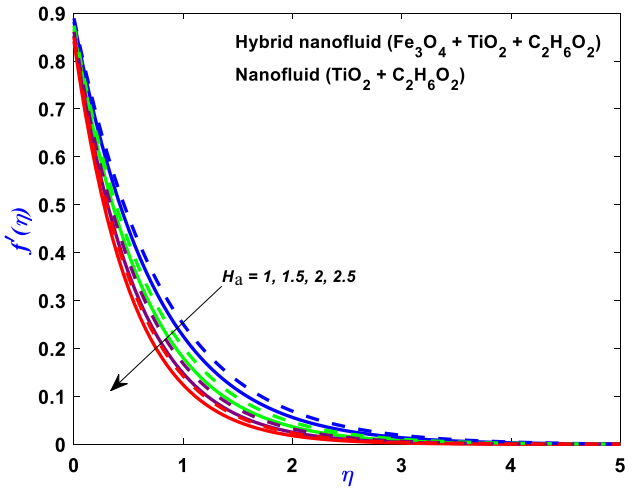


Fig. 2 Ha on $f'(\eta)$

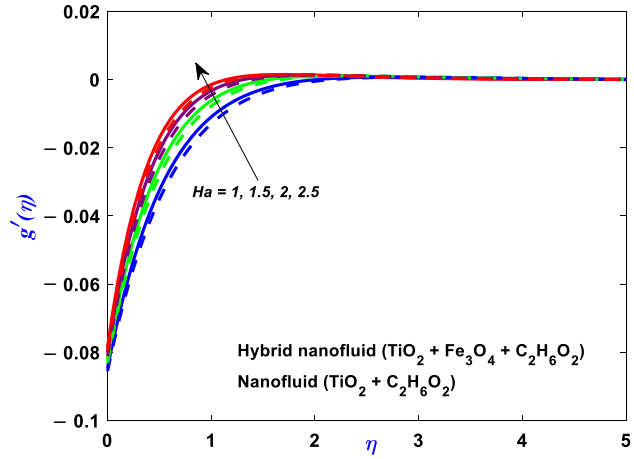


Fig. 3 Ha on $g'(\eta)$

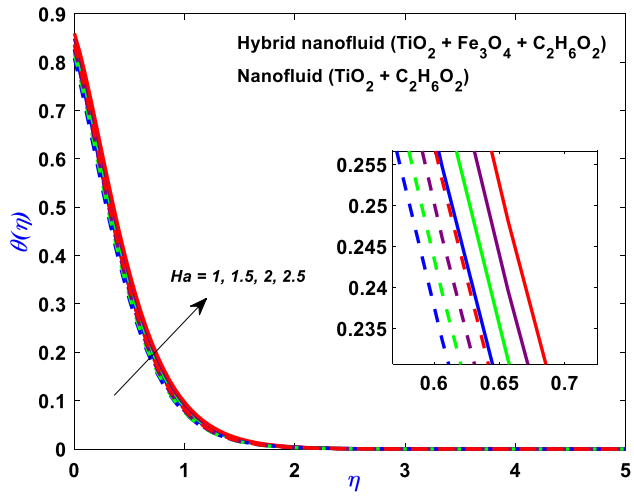


Fig. 4 Ha on $\theta(\eta)$

the earlier references. The fundamental thermal properties of the viscosity, conductivity, specific heat, etc., for the hybrid nanofluid is also depicted within the text. The mathematical model proposed for the said assumptions are designed and the transformations into non-dimensional form is presented by utilizing similarity rules. Further, shooting technique is adopted in finding the assumed initial guess values and then the Runge–Kutta method is employed in handling the solution of these equations. Table 2 presents the validation of the current result with the work of Xia et al. [22] for the particular values and it is seen that the coinciding results are well equipped which lead to the convergence policy of the methodology used. The significant characteristics of various factors affecting the flow phenomena are presented in the upcoming section.

Physical significance of Hall current

The flow profile consisting of both the axial and transverse velocity is affected by the implementation of the Hall current which shows the magnetized property on the flow profiles. Figures 2 and 3 depicts the impact of Hartmann number on the axial vis-à-vis transverse velocity and the results are constructed in two different folds. In particular, the case of $TiO_2 \sim$ EG nanofluid and $TiO_2 + Fe_3O_4 \sim$ EG hybrid nanofluid, respectively. To execute the variation, the Hartmann number (Ha) is considered as $1 \leq \text{Ha} \leq 2.5$. The generation of Lorentz force is produced for the involvement of Hall effect on the axial velocity and this resists the velocity profile which leads to a pronounced damping in the velocity distribution. Further, the comparative outcomes evident that with the inclusion of more nanoparticles that in the circumstances of bi-hybridized fluid the growing density, the attenuation in the profile is more pronounced. Moreover, in the transverse velocity the profile shows an augmentation in the distribution from the negative to positive direction for the increasing Hartmann number, as the magnitude escalates the profile thickness retards significantly due to the resistivity of the magnetization. Figure 4 portrays the attributes of the Hartmann number on the thermal state of fluid in contrast

to the variation of both the fluids. The diminished velocity across the flow domain stores energy at the bottom surface and this accumulated energy moves up and gives rise to an enhancement of the fluid's energy. Therefore, increasing Hartmann number enhances the fluid temperature irrespective of the fluids considered. In comparative analysis it is seen that for the hybridized fluid the fluid temperature is greater than that of the case of nanofluid. This fact is rendered due to the enhanced thermal conductivity of the hybrid nanofluid augments the fluid's energy. The profile is asymptotically meet the requisite surface conditions throughout.

Behavior of porosity

The transportation of hybridized fluid over an extending surface is embedded within the porous medium, give rise to project the effect of porosity on the flow profiles. Figures 5 and 6 depict the implication of the porosity on the axial and transverse velocity distribution, respectively. The results are presented for the considerable range of the factor Da as $0 \leq \mathrm{Da} \leq 3$. Here, the numerically assigned Da, $\mathrm{Da} = 0$ projects the insignificant role of porosity, i.e., the flow over a clear fluid medium and the $\mathrm{Da} \neq 0$ assigned for the flow through a permeable medium is shown. In a similar observation, porosity also provides a resistive force which leads to a significant resistive property to attenuates the axial velocity, and the profile shows a greater thickness in the velocity bounding surface. From the transverse velocity profile it is observe that increasing permeability overshoots the velocity in magnitude and the thickness retards significantly. In both the cases, the hybrid nanofluid with greater density retards the velocity bounding surface in comparison with the $TiO_2 \sim EG$ nanofluid. Figure 7 displays the role of Da on the fluid temperature of the hybrid

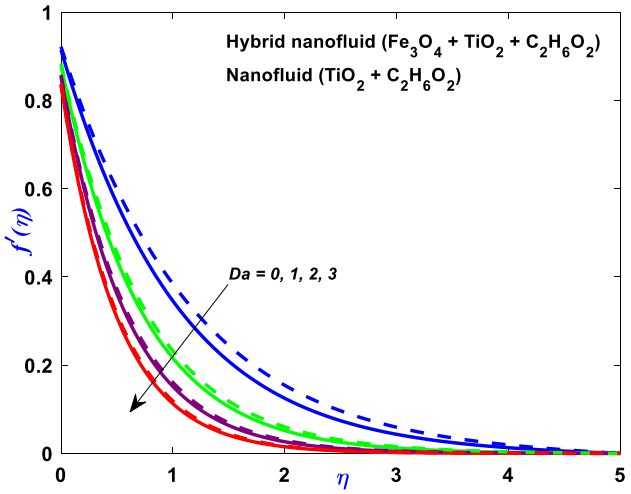


Fig. 5 Da on $f'(\eta)$

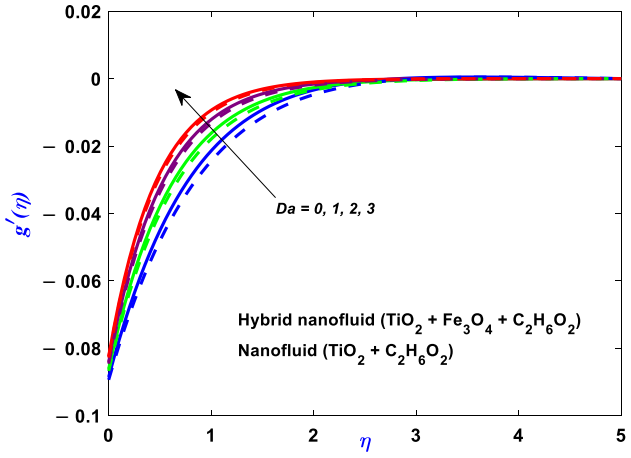


Fig. 6 Da on $f'(\eta)$

nanofluid. In similar observation, the heat transport phenomenon enhances greatly with the increasing porosity at all the points. The comparative analysis reveals that for the inclusion of more nanoparticles, i.e., the case of hybrid nanofluid with greater thermal conductivity encourages the heat transport properties and the fluid temperature increases greatly in comparison with the case of nanofluid.

Behavior of velocity slip

The velocity profile is affected due to the inclusion of velocity slip (K_1) on the profiles of axial and transverse velocity. Figures 8 and 9 display the implication of velocity slip affecting the profiles for the variation of single nanofluid and bi-hybrid nanofluid. The illustration of the factor is reported for the standard range of $0 \leq K_1 \leq 3$. Here, $K_1 = 0$ represents the no-slip constraints in which the velocity of the surface and the fluid motion at the surface

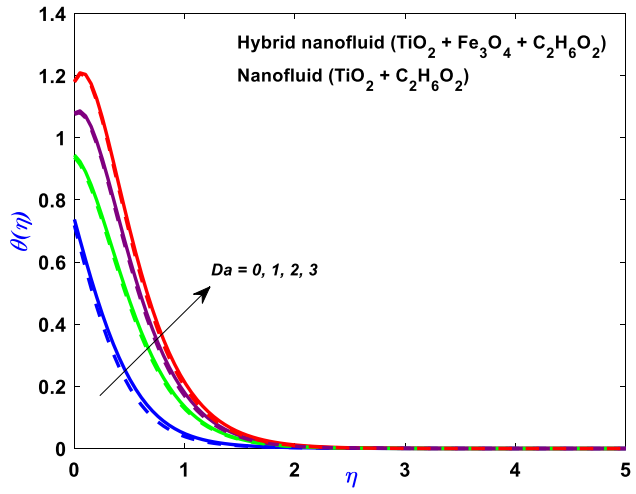


Fig. 7 Da on $\theta(\eta)$

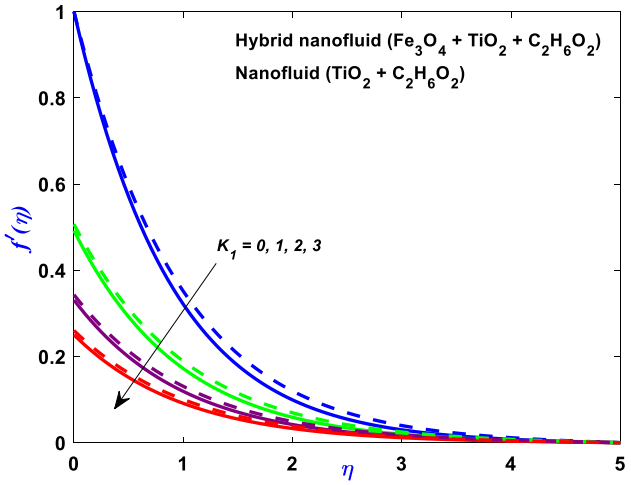


Fig. 8 K_1 on $f'(\eta)$

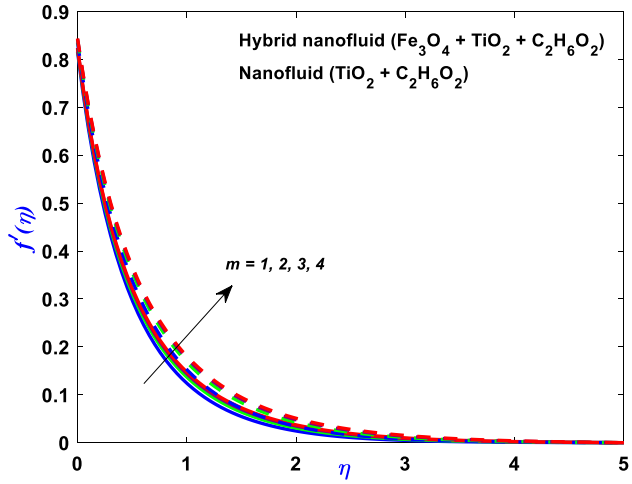


Fig. 10 K_1 on $g'(\eta)$

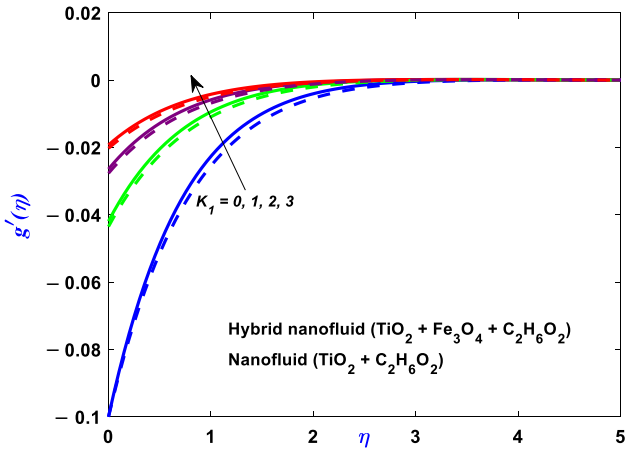


Fig. 9 K_1 on $g'(\eta)$

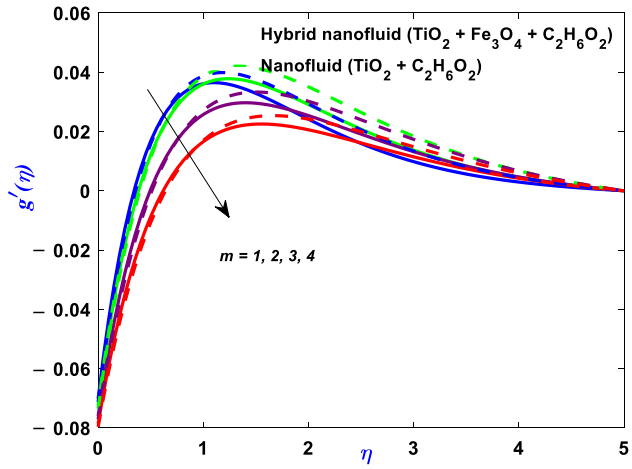


Fig. 11 m on $g'(\eta)$

are the same or zero. Further, the non-zero variation shows the behavior of slip where both velocities are different. In this case, the slip factor affects the fluid velocity significantly. From the figure it is observed that for the increasing slip the axial velocity attenuates throughout asymptotically and this causes a thinning in the velocity bounding surface thickness retards. Moreover, the transverse velocity distribution favors in elevating the profile for the increasing slip and as a result the thickness also retards. This behavior is rendered due to the greater density of the solid nanoparticles.

Effect of Hall current parameter

The interpretation of magnetization for the insertion of the Hall effect is projected in the flow profiles. Figures 10 and 11 showcase the contribution of the Hall current parameter on the axial and transverse velocity distribution. The consequence of the factor is reported by considering the range of the factor as $1 \leq m \leq 3$. As the magnetization retards the velocity profiles the electric current induced by the fluid momentum upserges the axial velocity and this enhancement is irrespective to the fluid considered. Further, the variation of the factor on the transverse velocity is reported corresponding to different fluids, such as single nanofluid and bi-hybrid nanofluid, respectively. The elevating Hall current parameter significantly enhances the profile thickness. Moreover, Fig. 12 depicts the behavior of the Hall current parameter on the temperature distribution of the hybrid nanofluid. The increasing Hall current favors in controlling the fluid's energy. In each of the distributions, i.e., for the velocity profile, the circumstances of hybrid nanofluid attenuate the fluid velocity in a greater rate whereas the case of fluid temperature, it augments the distribution in comparison with a single nanofluid. This

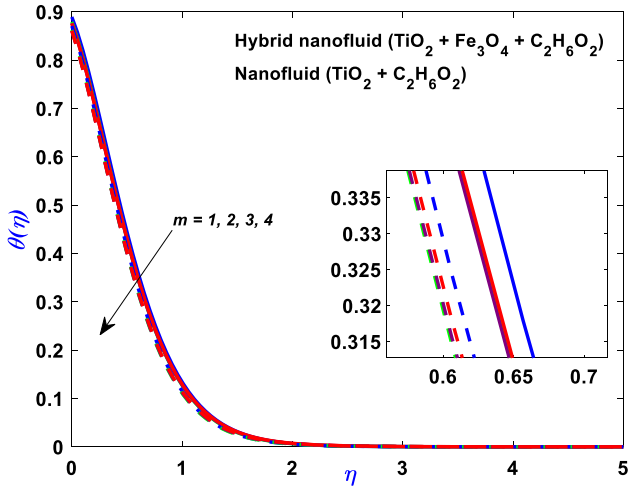


Fig. 12 m on $\theta(\eta)$

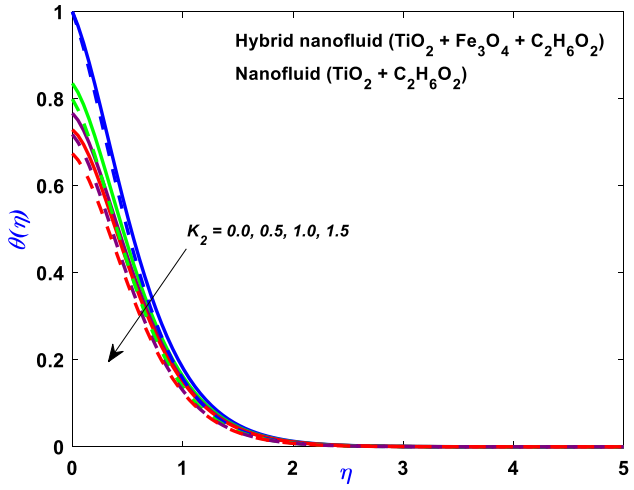


Fig. 14 K_2 on $\theta(\eta)$

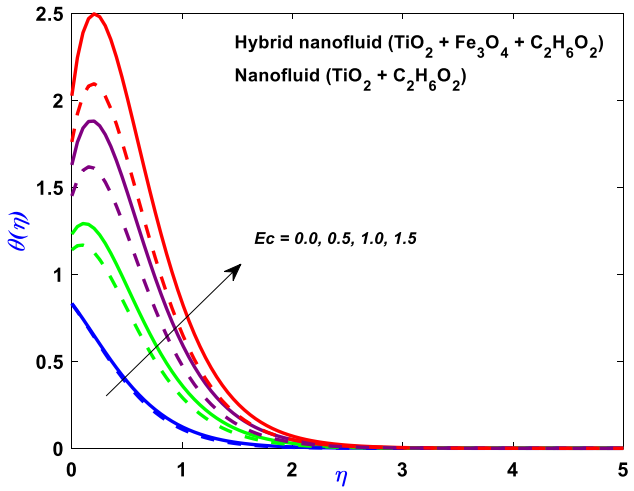


Fig. 13 Ec on $\theta(\eta)$

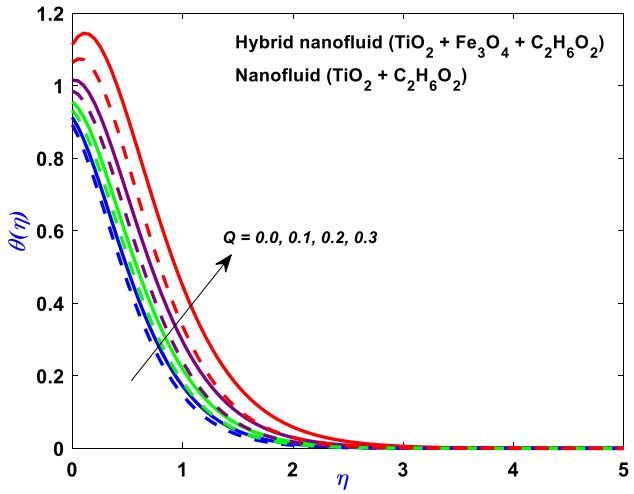


Fig. 15 Q on $\theta(\eta)$

behavior is executed due to the higher thermal conductivity of the nanofluid.

Behavior of Eckert number

The dissipative heat energy is assumed in the energy transport phenomenon for the consideration of both the Joule and Darcy dissipative heat. The Joule dissipation is inserted because of the magnetization property and the Darcy dissipation is encountered for the flow through permeable medium. Figure 13 describes the impact of Eckert number, the coupling parameter on the temperature distribution where the profile is presented in two-folds. The variation of the factor Ec is projected considering the range of the factor as $0 \leq \text{Ec} \leq 1.5$. Here, $\text{Ec} = 0$ assigned for the absence of dissipative heat whereas the non-zero value presents the behavior of Eckert number reflecting the dissipative heat impact. The factor is generally defined as the ratio of the kinetic energy and the enthalpy change. The increasing numerical values shows the increasing kinetic energy and vis-à-vis the retardation in the enthalpy. Physically, enthalpy is the difference between the temperature of the fluid and the ambient state temperature. The positive values indicates the greater temperature at the surface and therefore, the fluid temperature increases significantly. The comparative results presented from the figure that increasing thermal conductivity of the hybrid nanofluid for the inclusion of TiO_2 and Fe_3O_4 nanoparticles enhances the fluid temperature greatly than that of single nanofluid.

Table 3 Computation of skin fiction coefficient

Ha	Da	m	K_1	n	$(\mathrm{Re_x})^{0.5} Cf_x$		$(\mathrm{Re_x})^{0.5} Cf_y$	
					Hybrid nanofluid	Nanofluid	Hybrid nanofluid	Nanofluid
1					− 2.5797	− 1.8048	0.2284	0.2156
2					− 3.2219	− 2.2637	0.2948	0.2795
3					− 3.7118	− 2.6145	0.3428	0.3258
1	0.1				− 2.4454	− 1.6958	0.2237	0.2104
	0.2				− 2.5138	− 1.7514	0.2261	0.213
	0.3				− 2.5797	− 1.8048	0.2284	0.2156
	0.3	0.1			− 2.5797	− 1.8048	0.2284	0.2156
		0.2			− 2.5576	− 1.7885	0.2785	0.2634
		0.3			− 2.526	− 1.7654	0.3241	0.3069
		0.1	0.1		− 2.5797	− 1.8048	0.2284	0.2156
			0.2		− 2.2946	− 1.6177	0.1987	0.1891
			0.3		− 2.0681	− 1.4667	0.1758	0.1683
			0.1	0.1	− 2.5797	− 1.8048	0.2284	0.2156
				0.2	− 2.7533	− 1.919	0.2412	0.2272
				0.3	− 2.9246	− 2.0316	0.2537	0.2386

Behavior of thermal slip and heat source

The significant characteristic of the thermal slip due to the consideration of the convective condition and the impact of the heat source on the fluid temperature is depicted through Figs. 14 and 15, respectively. The parametric variation of the thermal slip (K_2) on the profile is conducted within the range of $0 \le K_2 \le 1.5$. Here, $K_2 = 0$ signifies a no-slip condition and $K_2 \neq 0$ indicates that the thermal slip is on the temperature profile. The increasing thermal slip retards the fluid temperature at all points within the domain. The comparative results are presented for the illustration of a single nanofluid and the hybrid nanofluid. Again, the enhanced thermal conductivity of the hybrid nanofluid for the inclusion of both nanoparticles encourages the heat transport phenomenon significantly, rather than the single nanofluid. Figure 15 demonstrates the characteristics of the heat source on the fluid temperature of the hybrid nanofluid. The behavior

Table 4 Computation of Nusselt number

Da	Ec	K_2	m	n	Q	$(\mathrm{Re_x})^{-0.5} Nu_x$	
						Hybrid nanofluid	Nanofluid
0.1						1.4137	1.5713
0.2						1.2475	1.3918
0.3						1.0891	1.2218
0.3	0.1					1.0891	1.2218
	0.2					0.5295	0.772
	0.3					− 0.0302	0.3223
	0.1	0.1				1.268	1.4304
		0.2				1.0891	1.2218
		0.3				0.9544	1.0663
		0.1	0.1			1.0891	1.2218
			0.2			1.1137	1.2445
			0.3			1.1386	1.2672
			0.1	0.1		1.0891	1.2218
				0.2		1.0059	1.1484
				0.3		0.9265	1.0792
				0.1	0.1	1.0891	1.2218
					0.2	0.8443	0.9877
					0.3	0.5413	0.7016

of the factor heat source Q is reported as $0 \leq Q \leq 0.2$. In general $Q = 0$ presents the absence of a heat source, which validates the case of earlier studies and the non-zero variation of heat source. The increasing heat source enhances the fluid temperature and the results are presented irrespective to the variation of the fluid considered. The result reveals that for the increasing particle concentration of nanoparticles in the hybrid nanofluid, enhances greatly in comparison with the single nanofluid.

The simulated results of the shear rate along both directions of the coordinate system is reported in Table 3. The behavior of distinct factors on the profile of skin friction coefficients is reported and it is seen that for the increasing Hartmann number and permeability, the skin friction coefficient enhances significantly, and the significant enhancement is observed due to the resistivity of the magnetization and the permeability of the medium. The increasing Hartmann number attenuates the shear rate profile which retards the skin friction coefficient. The behavior of velocity slip on the skin friction coefficient is presented. The result reveals that increasing velocity slip decelerates the skin friction coefficients and the increasing power index significantly enhances the coefficient. The comparative analysis reported that with the increasing particle concentration of the hybrid nanofluid enriches the profile.

Table 4 represents the characteristics of the heat transfer rate in the form of the Nusselt number for the variation of different factors. Here, the resistivity due to the inclusion of porosity retards the heat transfer rate so that the Nusselt number retards significantly. The increasing Eckert number retards the heat transfer rate and this retardation is the due to the retardation in the enthalpy. The increasing thermal slip attenuates the thermal gradient which favors in the retardation in the Nusselt number. However, the augmentation in the Hall current effect enhances the heat transfer rate. The increasing heat source controls the heat transfer rate and the Nusselt number decreases significantly.

Conclusions

A numerical investigation on the transportation of hybridized fluid comprising magnetized nanoparticles, i.e., Fe_3O_4 and the TiO_2, over the stretching surface embedded within the permeable medium is obtained in this article. The impact of dissipative heat, along with a heat source enriches the heat transport properties of the hybrid nanofluid. The transformed model, characterized by several factors, are handled numerically following similarity rules. Further, the physical behavior of various factors is presented and the important outcomes are displayed as;

- The numerical results presented in the tabular form show validation of the present result with the earlier investigation, and this leads to the convergence analysis of the present methodology.
- The magnetization due to the inclusion of the Hartmann number retards the axial velocity and the impact is opposite in case of transverse velocity.
- The velocity slip parameter significantly attenuates the thickness of the velocity bounding surface, and the results are depicted in both the case of single and bi-hybrid nanofluid.
- The heat transport phenomena elevate due to the inclusion of dissipative heat, i.e., the increasing Eckert number enhances the fluid temperature significantly.
- The shear rate profile is enhanced by the increasing magnetization, and this leads to develop the bounding surface thickness of the velocity boundary layer.
- The heat transfer rate is controlled by the increasing Eckert number, but the hybrid nanofluid enhances the rate in comparison with the case of the nanofluid.

Author contributions All the authors have equally contributed to complete the manuscript, i.e., SP has formulated the problem, FO has completed the introduction section and TMA checked the similarity with grammar, RB has computed and simulated the numerical results and finally, SRM have completed the draft with results and discussion section and checked the overall.

Funding Not applicable.

Data availability No data are used.

Code availability Not applicable.

Declarations

Conflict of interest The authors declare that they have no conflict of interest.

Ethics approval The entire work is the original work of the authors.

Consent to participate Not applicable.

Consent for publication All the authors have given their consent to publish the paper.

References

1. Almheidat M, Alqudah M, Souayeh B, Tuan NM, Ahmad S, Abualnaja KM. Nanoscale heat transport analysis of magnetized trihybrid nanofluid over wedge artery: Keller box and finite element scheme combination. Case Stud Therm Eng. 2024;64:105446.

2. Abderrahmane A, Mourad A, Mohammed S, Smaisim GF, Toghraie D, Koulali A, Younis O. Second law analysis of a 3D magnetic buoyancy-driven flow of hybrid nanofluid inside a wavy cubical cavity partially filled with porous layer and non-Newtonian layer. Ann Nucl Energy. 2023;181:109511.
3. Zhu Y, Zamani M, Xu G, Toghraie D, Hashemian M, Alizadeh AA. A comprehensive experimental investigation of dynamic viscosity of MWCNT-WO_3/water-ethylene glycol antifreeze hybrid nanofluid. J Mol Liq. 2021;333:115986.
4. Ibrahim SM, Kumar PV, Lorenzini G. Analytical modeling of heat and mass transfer of radiative MHD Casson fluid over an exponentially permeable stretching sheet with chemical reaction. J Eng Thermophys. 2020;29:136–55.
5. Reddy BP, Matao P, Sunzu JM. Finite element numerical investigation into unsteady MHD radiating and reacting mixed convection past an impulsively started oscillating plate. In: Defect and diffusion forum, vol. 401. Trans Tech Publications Ltd; 2020, pp. 47–62.
6. Li YX, Mishra SR, Pattnaik PK, Baag S, Li YM, Khan MI, Khan SU. Numerical treatment of time dependent magnetohydrodynamic nanofluid flow of mass and heat transport subject to chemical reaction and heat source. Alex Eng J. 2022;61(3):2484–91.
7. Zainal NA, Nazar R, Naganthran K, Pop I. Flow and heat transfer over a permeable moving wedge in a hybrid nanofluid with activation energy and binary chemical reaction. Int J Numer Meth Heat Fluid Flow. 2022;32(5):1686–705.
8. Almaneea A. Numerical study on heat and mass transport enhancement in MHD Williamson fluid via hybrid nanoparticles. Alex Eng J. 2022;61(10):8343–54.
9. Hussain Z, Muhammad S, Anwar MS. Effects of first-order chemical reaction and melting heat on hybrid nanoliquid flow over a nonlinear stretched curved surface with shape factors. Adv Mech Eng. 2021;13(4):1687814021999526.
10. Suneetha S, Reddy NB, Prasad VR. Thermal radiation effects on MHD free convection flow past an impulsively started vertical plate with variable surface temperature and concentration. J Nav Arch Mar Eng. 2008;5(2):57–70.
11. Ogulu A, Makinde OD. Unsteady hydromagnetic free convection flow of a dissipative and radiating fluid past a vertical plate with constant heat flux. Chem Eng Commun. 2008;196(4):454–62.
12. Tshivhi KS, Tshehla MS. Heat source and radiation effects on MHD flow of Copper–Water nanofluid over exponential stretching surface with slip. Results Phys. 2024;58:107463.
13. Sarma N, Paul A, Patgiri B. Computational study of Jeffrey hybrid nanofluid flow over on a non-uniformly heated permeable exponentially stretching surface with Arrhenius activation energy and inclined magnetic field. Hybrid Adv. 2024;6:100194.
14. Hamad MAA. Analytical solution of natural convection flow of a nanofluid over a linearly stretching sheet in the presence of magnetic field. Int Commun Heat Mass Transf. 2011;38(4):487–92.
15. Vinodkumar Reddy M, Ajithkumar M, Zafar SSB, Faizan M, Ali F, Lakshminarayana P. Magnetohydrodynamic stagnation point flow of Williamson hybrid nanofluid via stretching sheet in a porous medium with heat source and chemical reaction. In: Proceedings of the institution of mechanical engineers, part E: Journal of Process Mechanical Engineering, 09544089241239583. 2024.
16. Sharma RP, Mishra SR. A numerical simulation for the control of radiative heat energy and thermophoretic effects on MHD micropolar fluid with heat source. J Ocean Eng Sci. 2022;7(1):92–8.
17. Malik MY, Salahuddin T, Hussain A, Bilal S. MHD flow of tangent hyperbolic fluid over a stretching cylinder: using Keller Box method. J Magn Magn Mater. 2015;395:271–6. https://doi.org/10.1016/j.jmmm.2015.07.097.
18. Akbar NS, Nadeem S, Haq RU, Khan ZH. Numerical solutions of Magnetohydrodynamic boundary layer flow of tangent hyperbolic fluid towards a stretching sheet. Indian J Phys. 2013;87:1121–4. https://doi.org/10.1007/s12648-013-0339-8.
19. Idowu AS, Akolade MT, Abubakar JU, Falodun BO. MHD free convective heat and mass transfer flow of dissipative Casson fluid with variable viscosity and thermal conductivity effects. J Taibah Univ Sci. 2020;14:851–62. https://doi.org/10.1080/16583655.2020.1781431.
20. Gbadeyan JA, Titiloye EO, Adeosun AT. Effect of variable thermal conductivity and viscosity on Casson nanofluid flow with convective heating and velocity slip. Heliyon. 2020;6:e03076. https://doi.org/10.1016/j.heliyon.2019.e03076.
21. Reddy BS, Naik SHS. Radiation, absorption, and Joule heating influence on MHD Casson fluid flow over an exponentially stretching surface. Partial Differ Equ Appl Math. 2024;11:100790.
22. Xia WF, Ahmad S, Khan MN, Ahmad H, Rehman A, Baili J, Gia TN. Heat and mass transfer analysis of nonlinear mixed convective hybrid nanofluid flow with multiple slip boundary conditions. Case Stud Therm Eng. 2022;32:101893.

Publisher's Note Springer Nature remains neutral with regard to jurisdictional claims in published maps and institutional affiliations.

Springer Nature or its licensor (e.g. a society or other partner) holds exclusive rights to this article under a publishing agreement with the author(s) or other rightsholder(s); author self-archiving of the accepted manuscript version of this article is solely governed by the terms of such publishing agreement and applicable law.